Earth and Planetary Science Letters ∎ (∎∎∎∎) ∎∎∎–∎∎∎

Contents lists available at SciVerse ScienceDirect

Earth and Planetary Science Letters

journal homepage: www.elsevier.com/locate/epsl

Using centroid time-delays to characterize source durations and identify earthquakes with unique characteristics

Zacharie Duputel [a,*], Victor C. Tsai [a], Luis Rivera [b], Hiroo Kanamori [a]

[a] Seismological Laboratory, California Institute of Technology, Pasadena, CA, USA
[b] Institut de Physique du Globe de Strasbourg, UdS and EOST/CNRS UMR 7516, France

ARTICLE INFO

Article history:
Received 19 March 2013
Received in revised form
13 May 2013
Accepted 14 May 2013
Editor: P. Shearer

Keywords:
rupture duration
tsunami earthquakes
transform fault
scaling laws
earthquake source observations
seismicity and tectonics

ABSTRACT

The relationship between M_0 and the rupture duration is often difficult to establish. This is particularly true for large earthquakes for which the moment rate functions (MRF) generally have complicated shapes, and the estimated durations can vary considerably depending on the methodology used to evaluate the MRF. In this work, we show that the centroid time-delay (τ_c) provides an alternative estimate of the source duration. Inverted MRFs often end gradually, making the end of coseismic rupture difficult to detect. In such cases, when the rupture duration is not well defined, the time-delay τ_c is a useful quantity to represent the first-order temporal characteristics of the rupture process. Variations in stress parameter $\Delta\sigma$ can be investigated by assuming a standard scaling relationship between the seismic moment M_0 and τ_c. This simple scaling relationship can also be used to identify unusual earthquakes, with unique source properties, such as events involving complicated rupture processes or earthquakes characterized by unusual rupture velocities, stress drops or aspect ratios.

1. Introduction

Scaling relations are often used in seismology to understand basic and common properties of the seismic source (Kanamori and Anderson, 1975). One of the most commonly used relationships is that between seismic moment (M_0) and rupture dimension (e.g., Aki, 1972; Romanowicz, 1992; Scholz, 1982), which can in turn be used to estimate common source properties (e.g., the stress drop). However, source dimensions are usually only indirectly estimated which can cause considerable uncertainties in the estimated source properties. Several studies have also focused on the link between M_0 and the corner frequency (f_c) of small earthquakes (e.g., Aki, 1967; Shearer et al., 2006). In such analyses, it is common practice to use seismic moment and corner frequency (f_c) measurements to estimate an average stress drop ($\Delta\sigma$). This estimate usually requires a number of assumptions about the source, such as the shape of the faulting area or the average rupture velocity (e.g., Brune, 1970). The resulting stress drop estimates usually vary over several orders of magnitude (Allmann and Shearer, 2009) and we may ask if this scatter is real or is a consequence of incorrect assumptions about the source model and of uncertainties in f_c estimates. Despite this variability in stress drop measurements, corner frequency observations are of primary importance as they contribute to various ongoing debates about earthquake self-similarity and regional variations of source properties. These analyses are, however, more difficult to conduct for large earthquakes (i.e., $M_w \geq 6.5$), partly because source complexity is more apparent as magnitude increases.

Long-period seismology is a robust tool to characterize elastic structure (Dziewonski and Anderson, 1981) and quantify source parameters of earthquakes (Dziewonski et al., 1981; Kanamori and Given, 1981). With the advent of broad-band instrumentation (Wielandt and Steim, 1986; Wielandt and Streckeisen, 1982) and the expansion of global seismological networks, long-period observations today provide some of the most robust information on the characteristics of large earthquakes. In particular, we can now determine the relationship between M_0 and the source duration objectively and directly from seismograms. In this short note, we show that the centroid time-delay (τ_c) estimated from long-period source inversion provides a very straightforward and reliable estimate of the rupture duration. A scaling relation between the seismic moment M_0 and the centroid time-delay τ_c is discussed on the basis of an extensive set of earthquake data, including all events of $M_w \geq 6.5$ between 1990 and 2012. This scaling relation is used to study the relative variation of source properties and identify events with unique source characteristics.

2. Centroid time-delay measurements

Source inversion approaches such as the Global CMT (GCMT) or the W-phase source inversion algorithm (WCMT) use a very simple parameterization of the source with a small number of parameters

* Corresponding author. Tel.: +1 626 395 3801.
E-mail address: zacharie@gps.caltech.edu (Z. Duputel).

0012-821X/$ - see front matter © 2013 Elsevier B.V. All rights reserved.
http://dx.doi.org/10.1016/j.epsl.2013.05.024

to be determined (Dziewonski et al., 1981; Kanamori and Rivera, 2008). The source is assumed to be a point source in space, with an isosceles-triangular moment rate function (MRF). The source parameters to be determined are then the elements of the seismic moment tensor, the point-source space–time coordinates (latitude, longitude, depth, time at the center of the MRF) and the rupture half-duration (i.e., half-width of the triangular MRF).

We use two catalogs that provide the point-source parameters of worldwide earthquakes of $M_w \geq 6.5$ between 1990 and 2012. The first catalog contains the WCMT solutions provided by Duputel et al. (2012) for 1990–2010 earthquakes (available at the url http://wphase.unistra.fr). We extended this catalog to 2011–2012 events using the same procedure. The second catalog is built with the GCMT solutions between 1990 and 2012 (Ekström et al., 2012; also available at the url: http://www.globalcmt.org). To focus on well-constrained point-source parameters, we rejected events whose signals are contaminated by large amplitude waveforms of a preceding event. These earthquakes, defined as "disturbed events" in Duputel et al. (2012), are listed in the Online Supplementary Information. Fig. 1a compares the moment magnitude estimates from the GCMT and WCMT catalogs for all events between 1990 and 2012. The reliability of such catalogs is well illustrated here with an absolute magnitude deviation smaller than 0.2 for 99% of the events.

The half-duration τ_h is generally poorly constrained in CMT inversions because of the long-period character of the waveforms used in these methods (i.e. periods of 40–350 s for GCMT, 100–1000 s for WCMT). In fact, in GCMT inversions, an empirical scaling between half-duration and seismic moment M_0 is assumed to set τ_h (Dziewonski and Woodhouse, 1983; Ekström, 1989; Ekström and Engdahl, 1989). The centroid time, on the other hand, is generally well constrained. In this study, we use the centroid time-delay τ_c as a proxy for the half-duration τ_h of the event. This assumption is explicitly used in the WCMT algorithm in which we assume $\tau_h = \tau_c$ after estimating τ_c. The time-delay, τ_c, is the difference between the MRF center time and the rupture nucleation time (i.e. the origin time). As we will see in the next section, the assumption $\tau_c = \tau_h$ is reasonable as long as the origin time, which is generally determined from body-wave travel-times, is accurate. The raw τ_c values in GCMT and WCMT solutions are generally given with respect to preliminary estimates of the origin time, which can be affected by large errors. To improve our measurements, we thus updated the time-delays τ_c using the origin times from the final USGS PDE catalog. Fig. 1b compares the resulting estimates from GCMT and WCMT catalogs for all events between 1990 and 2012. The total set of τ_c measurements is given in Table S2 of the Online supplementary information. Time-delays are compared with rupture duration estimates in the next section.

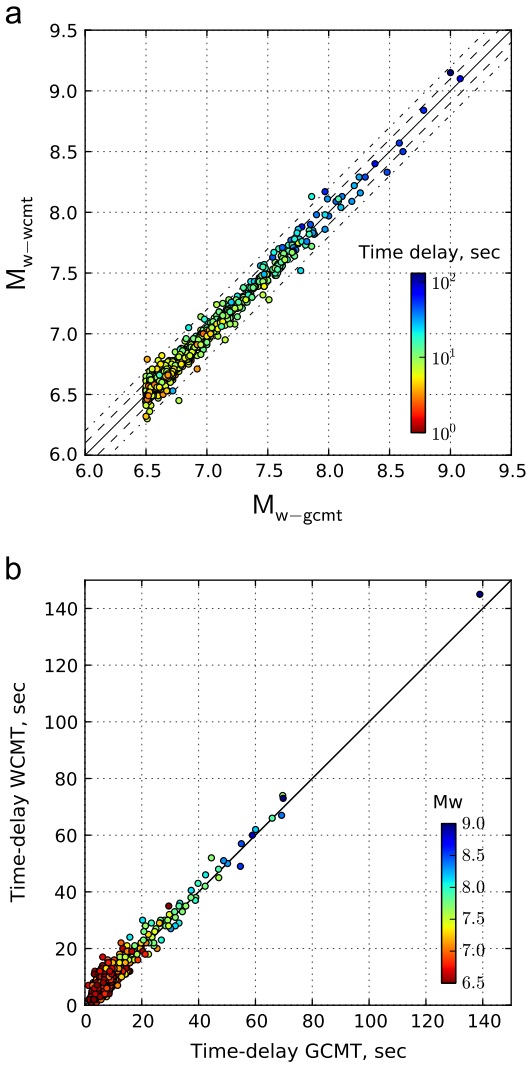

Fig. 1. An illustration of the consistency between GCMT and WCMT catalogs. (a) Comparison of moment magnitude estimates from the WCMT (M_{w-wcmt}) and GCMT (M_{w-gcmt}) catalogs. Symbols are colored according to the GCMT centroid time-delay. Dashed lines indicate ± 0.1 and dot-dashed lines ± 0.2 magnitude units. (b) Comparison of centroid time-delay estimates from WCMT and GCMT catalogs. Symbols are colored according to the GCMT moment magnitude. (For interpretation of the references to color in this figure legend, the reader is referred to the web version of this article.)

3. Comparison between centroid time-delay and rupture duration

The source duration, τ_d, is given by $\tau_d = t_e - t_0$ where t_0 is the time when the rupture on the fault begins (i.e. the origin time) and t_e is when the co-seismic slip motion ends. For the widely used Haskell model, $t_e = t_0 + L/V + \tau$ where L is the unilateral rupture length, V is the rupture speed, and τ is the rise-time of local slip function. The moment rate function (MRF) for this source is given by a trapezoid with a rise and fall time of τ, and a top flat portion of duration $L/V - \tau$. The rupture duration, τ_d, is usually determined from the MRF, $m(t)$, determined as part of the slip inversion using seismic waves.

On the other hand, the centroid time-delay is given by $\tau_c = \int (t - t_0)\, m(t)\, dt / \int m(t)\, dt$, where the time integrals are taken over the entire MRF. In GCMT and WCMT analyses, $m(t)$ is assumed to be an isosceles triangle and the time at the center of the triangle (i.e., the centroid time t_c) is determined by inversion. The origin time, t_0, is determined from high-frequency P-wave arrival times. If the centroid time-delay ($\tau_c = t_c - t_0$) is accurately determined, the source duration (τ_d) can be estimated by $\tau_d = 2\tau_c$. This assumption is reasonable since, for most earthquakes, $m(t)$ is well approximated by a symmetrical triangle, trapezoid, or a single sinusoid (e.g., 2010 Maule earthquake; 2011 Tohoku-oki earthquake; Lay and Kanamori, 2011).

Fig. 2a shows a comparison between GCMT and WCMT centroid time-delays and rupture duration measurements provided in the literature. We see that there is an overall consistency between duration and time-delay measurements. The centroid time-delay (τ_c) is a very straightforward observable and there is good agreement between τ_c measurements estimated from the GCMT and from the WCMT catalogs. This indicates a small uncertainty for τ_c, as expected for long-period robust CMT inversion techniques. In general, as long as the time-smoothed $m(t)$ is relatively simple and symmetric around the center, then $\tau_d = 2\tau_c$ is a good

Please cite this article as: Duputel, Z., et al., Using centroid time-delays to characterize source durations and identify earthquakes with unique characteristics. Earth and Planetary Science Letters (2013), http://dx.doi.org/10.1016/j.epsl.2013.05.024

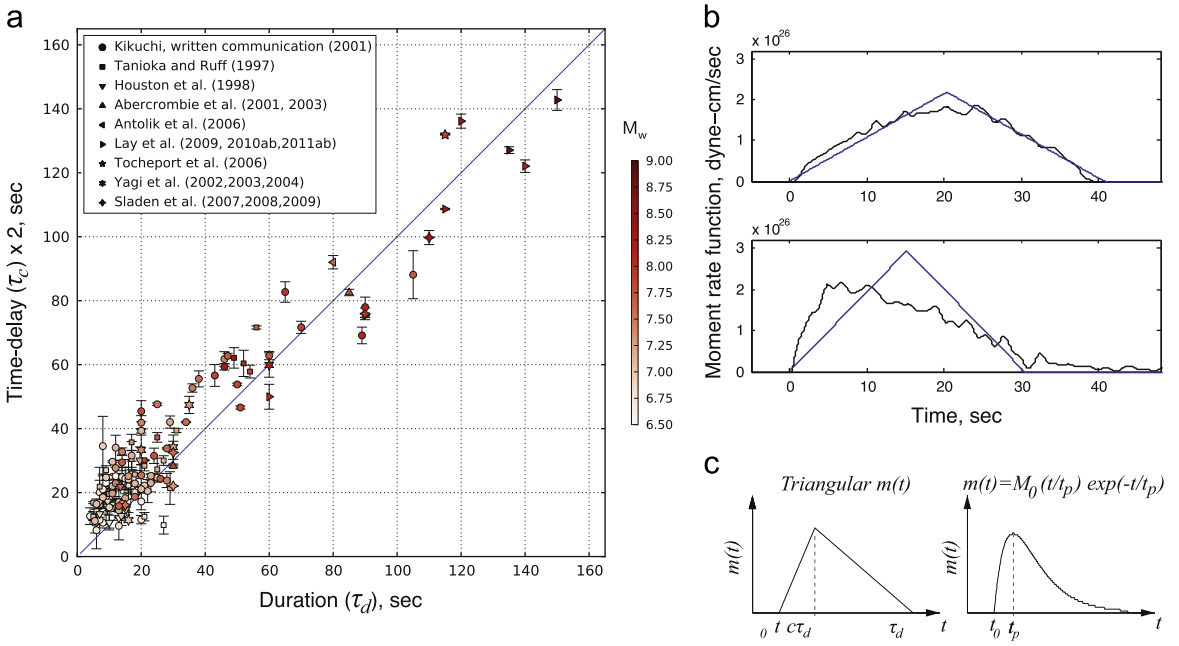

Fig. 2. Comparison between centroid time-delay (τ_c) and rupture duration (τ_d). (a) Rupture duration measurements provided in the literature for $M_w \geq 6.5$ earthquakes are compared with duration estimated from our time-shift measurements (Abercrombie et al., 2003, 2001; Antolik et al., 2006; Houston et al., 1998; Lay et al., 2011, 2010a, 2010b; Lay and Kanamori, 2011; Lay et al., 2009; Sladen, 2009a, 2009b, 2008a, 2008b, 2007a, 2007b; Kikuchi, written communication, 2001; Tanioka and Ruff, 1997; Tocheport et al., 2006; Yagi, 2004, 2003, 2002). Error bars represent the deviation between GCMT and WCMT measurements for each earthquake (the symbols correspond to the average time-shift). (b) Illustrations of moment rate functions (MRF, $m(t)$) for a triangular $m(t)$ (left) and $m(t) = M_0\,(t/t_p)\exp(-t/t_p)$ (right). (c) Examples of time-shift measurement for synthetic MRF with different shapes. The time-shift is measured at the center of the isosceles triangle (blue) that best fit the MRF (black). (For interpretation of the references to color in this figure legend, the reader is referred to the web version of this article.)

approximation as illustrated in Fig. 2b. The time-delay τ_c at the center of the best-fitting triangle is thus a fairly effective and straightforward estimate of the rupture duration. On the other hand, the rupture duration estimates (τ_d) can be somewhat ambiguous. The MRFs often end gradually and in such cases, the rupture duration end (t_e) can be difficult to detect as shown in Fig. 2b (bottom). In such situations, when the rupture duration is not well defined, the time-delay τ_c is probably a more appropriate quantity to represent the average temporal characteristics of the rupture process.

There are exceptions, however, such as the 2004 Sumatra–Andaman Is. earthquake ($M_w = 9.2$). For this event, the MRF has a very long tail and $\tau_d \approx 3.5\tau_c$ instead of $\tau_d = 2\tau_c$ ($\tau_c = 139$ s from GCMT inversion and $\tau_c = 145$ from WCMT). Assuming that the source time function $m(t)$ is a simple triangle with a duration τ_d and a maximum amplitude at a time $c{\cdot}\tau_d$, Fig. 2c (left) illustrates a schematic MRF of the Sumatra–Andaman Is. earthquake. In this case, we have a centroid time-delay given by $\tau_c = \tau_d(1+c)/3$. We can also assume a long tailed MRF of the form $m(t) = M_0(t/t_p)\exp(-t/t_p)$ as shown in Fig. 2c (right) with a centroid time-delay of $\tau_c = 2t_p$. For the 2004 Sumatra–Andaman Is. earthquake, the MRF is not determined very well, which leads to a large variability of duration estimates between 400 s and 600 s. If we take $\tau_d = 500$ s, $c = 0.2$, $t_p = 100$ s from Ammon et al. (2005), τ_c should be about 200 s (i.e. $\tau_d \approx 2.5\tau_c$), which is still larger than WCMT and GCMT measurements (i.e., $\tau_d \approx 3.5\tau_c$). This event can, however, be considered as a very extreme case and $\tau_d = 2\tau_c$ can be considered as a good assumption for most earthquakes.

4. Absolute time-delay anomalies

In this section, we examine the difference between centroid time-delay measurements τ_c and predictions from scaling laws. This comparison is interesting because it allows for the identification of anomalous earthquakes for which measurements and predictions significantly differ. The scaling relation used in WCMT inversions for the initial half-duration is (Duputel et al., 2012):

$$\tau_r = 1.2 \times 10^{-8} \times {M_0}^{1/3} \quad (1)$$

In this study, τ_r is a reference half-duration predicted for a given seismic moment M_0 (in dyne-cm). Fig. S1 in the Online Supplementary Information shows a comparison between rupture duration measurements (τ_d) and a scaling half-duration (τ_r). There are significant differences between τ_d and $2\tau_r$, unlike the general agreement between τ_d and $2\tau_c$ shown in Fig. 2. This indicates that rupture duration anomalies can be detected by looking at the difference $\Delta\tau = \tau_c - \tau_r$ between time-delay measurements τ_c and scaling predictions $\tau_r = 1.2 \times 10^{-8} \times M_0^{1/3}$. The values of $\Delta\tau$ are shown in Fig. 3 for all the events with $M_w \geq 6.5$ in chronological order for the period 1990–2012. Approximately 95% of the events are within ± 10 s, indicating that this scaling relationship represents the general behavior of moderate to large earthquakes. However, $\Delta\tau$ loses its significance for small earthquakes since it is generally small regardless of the source characteristics (e.g., $M_w \leq 7.1$ earthquakes have half-durations $\tau_r < 10$ s).

Here we focus on the events for which $\Delta\tau$ significantly deviates from 0. These earthquakes do not strictly follow the scaling relation, which suggests that each of them has unique source properties. Rupture duration anomalies can be interpreted as the result of (1) abnormal rupture or slip velocities, (2) stress-drop variations, (3) atypical fault geometries, or (4) complicated faulting processes (e.g., rupture partitioning in several subevents). Although measuring $\Delta\tau$ alone does not allow us to distinguish between these different possibilities, it provides a robust and straightforward way to identify events with peculiar characteristics.

Fig. 3 clearly shows that the two largest events of the 1990–2010 time-period have unique temporal characteristics. The 2004 $M_w = 9.2$ Sumatra–Andaman Is. earthquake has a large value of $\Delta\tau$. With a rupture duration of about 500 s, this event is indeed

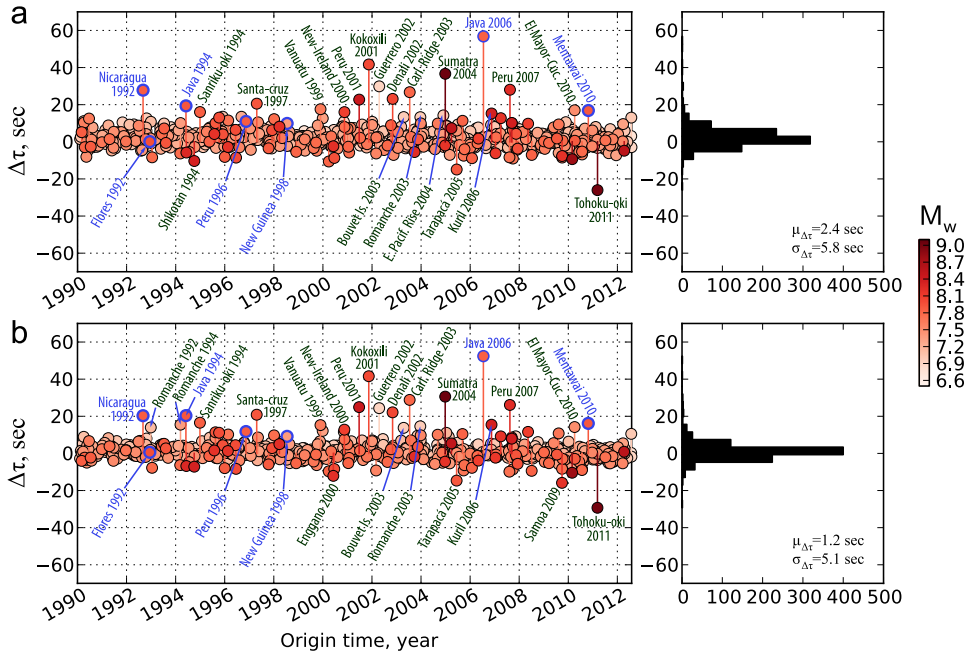

Fig. 3. Time-delay difference $\Delta\tau = \tau_c - \tau_r$ between measurements τ_c and predictions $\tau_r = 1.2 \times 10^{-8} \times M_0{}^{1/3}$ for the events which occurred during the period from January 1990 to September 2012. (a) Time-delays from the W phase catalog. (b) Time-delays from the Global CMT catalog. Tsunami earthquakes are highlighted in blue. Mean ($\mu_{\Delta\tau}$) and standard deviation ($\sigma_{\Delta\tau}$) of the $\Delta\tau$ distributions are shown on the histograms for both catalogs. (For interpretation of the references to color in this figure legend, the reader is referred to the web version of this article.)

the earthquake with the longest duration ever observed in the history of instrumental seismology (Ammon et al., 2005; Ishii et al., 2005; Lambotte et al., 2006; Tsai et al., 2005). On the other hand, the 2011 $M_w = 9.0$ Tohoku-oki earthquake is associated with a small $\Delta\tau$ and thus stands out as a very temporally compact event (Lay and Kanamori, 2011). Other earthquakes with high-stress drop can also be identified such as the $M_w = 8.2$ 1994 Shikotan event (Kikuchi and Kanamori, 1995) and the $M_w = 7.7$ 2005 Tarapacá earthquake (Kuge et al., 2010). Although the 2004 Sumatra–Andaman Is. and the 2011 Tohoku-oki earthquakes stand out because of their large absolute time-delay difference $|\Delta\tau| = |\tau_c - \tau_r|$ (i.e., $|\Delta\tau| > 20$ s), we note that the corresponding relative difference $|\Delta\tau|/\tau_r$ remains small because of the long duration expected for such large magnitude events (i.e., $|\Delta\tau|/\tau_r \leq 0.3$).

Another set of events that we can easily identify includes tsunami earthquakes. Defined initially by Kanamori (1972), these events produce unusually large tsunamis relative to their radiated seismic energy (Newman and Okal, 1998). They are currently interpreted as either having an anomalously slow rupture process or as being accompanied by underwater landslides and slumping. Events previously identified as tsunami earthquakes in the literature are highlighted in blue in Fig. 3. Four of them can be easily identified as $\Delta\tau$ outliers:

(1) The first one is the 1992 Nicaragua earthquake ($M_w = 7.6$), which is a slow thrust event that probably occurred close to the middle America trench (Kanamori and Kikuchi, 1993; Satake, 1994).
(2) The second outlier is the 1994 Java earthquake ($M_w = 7.8$). This event has a number of unusual characteristics and was a matter of debate in the literature. Abercrombie et al. (2001) argued that there is no evidence for slow and shallow rupture and interpreted the deficiency in high frequency as due to low average stress drop (~0.3 MPa). On the other hand, Polet and Thio (2003) proposed that it had a slow rupture velocity and/or a slow slip velocity.
(3) The third event is the 2006 Java earthquake ($M_w = 7.7$) that has the largest $\Delta\tau$ anomaly of the 1990–2012 time-period. It is a classic example of a tsunami earthquake, with slow rupture velocity and large slip distributed close to the trench (Ammon et al., 2006).
(4) The last one is the 2010 Mentawai earthquake ($M_w = 7.8$), for which the large value of $\Delta\tau$ is consistent with studies reporting a slow rupture process (Hill et al., 2012; Lay et al., 2011; Newman et al., 2011).

Some tsunami earthquakes, such as the 1992 Flores earthquake ($M_w = 7.7$) and the 1998 Papua-New-Guinea earthquake ($M_w = 7.0$), do not appear to have anomalously long rupture durations. This is consistent with observations from Polet and Kanamori (2000) indicating no particular high-frequency deficiency in the spectrum of these events. The unusually large tsunami amplitudes for these earthquakes can probably be explained by slumping or underwater landslides as suggested for the Flores event by Tsuji et al. (1995) and Hidayat et al. (1995), and for the Papua-New-Guinea earthquake by Heinrich et al. (2000) and Synolakis et al. (2002). For the 1996 Peru event ($M_w = 7.5$), the value of $\Delta\tau$ shows that the earthquake had a long duration but does not quite belong to the class of slow tsunami earthquakes (Ihmlé et al., 1998).

Although not classified as tsunami earthquakes, other events with anomalously long rupture duration can also be identified:

(1) The 1994 Sanriku-oki earthquake ($M_w = 7.7$) is an interesting event with very large after-slip that lasted for about a year (Heki et al., 1997). The long duration indicated by the large value of $\Delta\tau$ is consistent with a slow rupture initiation stage observed by Tanioka et al. (1996) and Nakayama and Takeo (1997).
(2) The long duration of the 1997 Santa Cruz earthquake ($M_w = 7.8$) is also consistent with observations from Kaverina

et al. (1998) that reported a low rupture velocity of about 1.9 km/s.

(3) Another very interesting event is the April 18, 2002 Guerrero earthquake ($M_w = 6.7$), for which the estimated time-delay ($\tau_c \sim 30$ s) is nearly five times longer than what is expected from the scaling relation. This event can be interpreted as an aftershock of the large $M_w \sim 7.5$ slow-slip event in 2001–2002 and is deficient in high-frequency energy (Iglesias et al., 2003; Kostoglodov et al., 2003). This last observation, as well as the centroid location being close to the trench with the generation of a tsunami (which is quite surprising for such a small event), suggests a small tsunami earthquake-like event.

As proposed above, events with a complicated rupture process may also display abnormal time-delay values. Good examples are the $M_w = 7.9$ 2001 Kokoxili earthquake, the $M_w = 7.9$ 2002 Denali event and the $M_w = 7.2$ 2010 El Mayor–Cucapah earthquake (Eberhart-Phillips et al., 2003; Hauksson et al., 2010; Tocheport et al., 2006). These events are made of several subevents that involve large moment rate at a significant delay with respect to the origin time. Similarly, the rather long durations observed for the Peru earthquakes in 2001 ($M_w = 8.4$) and 2007 ($M_w = 8.0$), may be interpreted as a result of rupture partitioning into two subevents as reported by Sladen et al. (2010) and Lay et al. (2010a). Regarding the $M_w = 8.0$ 2000 New-Ireland earthquake, the large observed time-delays can probably be explained by the obvious source complexity of this event. This earthquake shows large differences between point-source and finite-fault inversion results (Duputel et al., 2012) and the occurrence of a late dip-slip subevent was also proposed (Earthquake Research Institute (ERI), 2000; Park and Mori, 2007). In a similar way, the small value of $\Delta\tau$ obtained by GCMT analysis for the 2009 Samoa earthquake can be seen as a consequence of its remarkable source complexity with two subevents having nearly opposite mechanisms (Lay et al., 2010c). The same interpretation can be made for the $M_w = 7.9$ 2000 Enggano earthquake that involved a combination of two subevents with strike-slip and thrust mechanisms (Abercrombie et al., 2003). The Samoa and Enggano earthquakes showed large differences between GCMT and WCMT solutions (Duputel et al., 2012) as well as important variations in estimated time-delays. This suggests that a single-point-source representation is not suitable for these events and that the estimated time-delays may therefore not be completely relevant.

Other events that stand out include oceanic fracture zone earthquakes such as the 2003 Carlsberg ridge earthquake ($M_w = 7.6$). The large value of $\Delta\tau$ that we obtained for this event is consistent with the long rupture duration observed by Antolik et al. (2006). Similar but smaller oceanic fracture zone earthquakes can also be identified in Fig. 3. These are the 2003 Bouvet Is. earthquake (April 17, $M_w = 6.5$), the 2004 East Pacific Rise event (November 28, $M_w = 6.6$) and the Romanche earthquakes in 1992 (December 26, $M_w = 6.8$), 1994 (March 14, $M_w = 7.0$) and 2003 (December 21, $M_w = 6.5$). As a result of their small magnitudes and associated time-delays, these earthquakes do not clearly stand out in Fig. 3. The discrepancies between measured (τ_c) and predicted (τ_r) time-delays for these events are discussed more in detail in the next section where we look at the normalized time-delay τ_c/τ_r.

5. Relative time-delay anomalies

In Fig. 3, time-delay anomalies are not scaled by event sizes. Thus, for small earthquakes, $\Delta\tau = \tau_c - \tau_r$ is generally small regardless of the source characteristics of the events. In other words, differences in source characteristics for small earthquakes do not show up in Fig. 3 (except for the $M_w = 6.7$ 2002 Guerrero earthquake on April 18). Moreover, if we use $\Delta\tau$ as a variable, the distribution of time-delay anomalies is necessarily asymmetrical. Indeed, because of the time-delay positivity $\tau_c > 0$ and $\tau_r > 0$, there is a lower bound $\Delta\tau > -\tau_r$. This asymmetry in the distribution of $\Delta\tau$ will highlight events with long durations and de-emphasize temporally compact earthquakes. For instance, if we assume a $M_w = 7.7$ event, we have a prediction $\tau_r = 20$ s from Eq. (1) and the minimum expected time-delay anomaly will be $\Delta\tau_{min} = -20$ s. On the other hand, $\Delta\tau$ can be very large such as for the $M_w = 7.7$ 2006 Java earthquake, for which we have $\Delta\tau \approx 55$ s. To obtain a symmetrical distribution of time-delay anomalies, in this section we focus on the difference between the logarithms of τ_c and τ_r, i.e., $\log(\tau_c/\tau_r)$.

As discussed above, an alternative way to show the scaling relation is to scale τ_c by τ_r, and plot $\tau_c/\tau_r = \tau_c/(1.2 \times 10^{-8} \times M_0^{1/3})$ on a logarithmic scale as a function of M_0. Fig. 4 shows τ_c and τ_c/τ_r as a function of M_0 for all $M_w \geq 6.5$ earthquakes from 1990 to 2012. As expected, we notice that the distribution of τ_c/τ_r on a log-scale is much more symmetrical than that of $\Delta\tau$ in Fig. 3a and b. It has been observed, however, that τ_c has a small (1–2 s) bias towards positive values (Dziewonski and Woodhouse, 1983), perhaps due to the different Earth models used by USGS PDE and GCMT catalogs (Smith and Ekström, 1995). To test the effect of this bias, in Fig. S2, we plot the same τ_c/τ_r as in Fig. 4 but account for a 1 s offset. As shown, there is no significant difference between Fig. S2 and Fig. 4, although small shifts are visible for the smallest events.

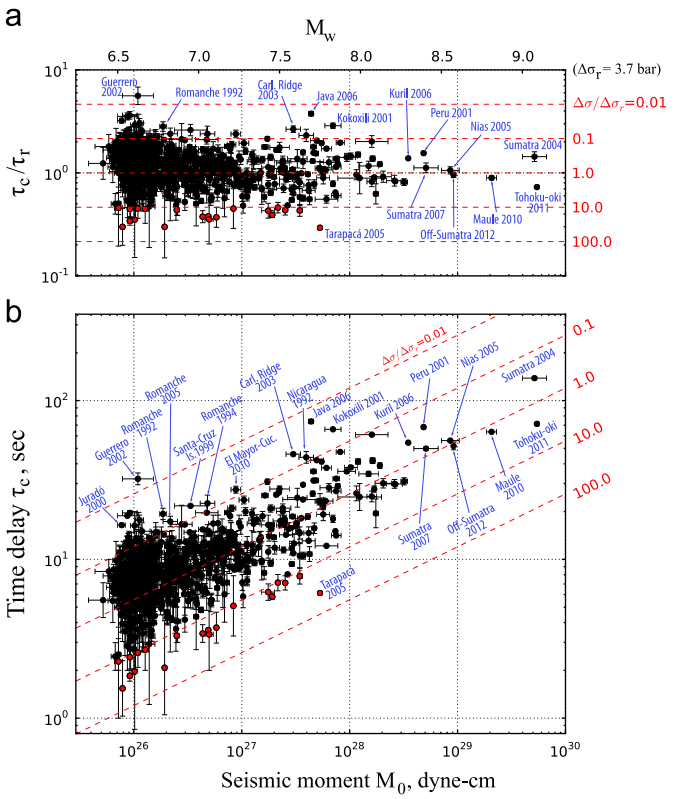

Fig. 4. Ratios τ_c/τ_r of observed time-delays τ_c to predictions $\tau_r = 1.2 \times 10^{-8} \times M_0^{1/3}$ for the events which occurred during the period from 1990 to 2012. (a) Relative time-delays τ_c/τ_r and (b) measured time-delays τ_c are shown as a function of the seismic moment. Black circles correspond to the geometric mean between GCMT and WCMT observations while error bars represent the deviation between GCMT and WCMT measurements for each earthquake. Stress parameter ratios $\Delta\sigma/\Delta\sigma_r$ obtained assuming a reference $\Delta\sigma_r = 3.7$ bars are presented on each graph. Red circles indicates events for which $\Delta\sigma/\Delta\sigma_r > 10$ (also shown in Fig. 5). Event names are given for obvious τ_c/τ_r outliers and large events. Earthquakes with large τ_c/τ_r values that are not named for $M_0 < 2{\cdot}10^{26}$ dyne-cm, are identified in Fig. 6. (For interpretation of the references to color in this figure legend, the reader is referred to the web version of this article.)

Please cite this article as: Duputel, Z., et al., Using centroid time-delays to characterize source durations and identify earthquakes with unique characteristics. Earth and Planetary Science Letters (2013), http://dx.doi.org/10.1016/j.epsl.2013.05.024

In the following, we will therefore focus only on the raw time-delay measurements presented in Fig. 4. Notice that for smaller earthquakes ($M_w \leq 6.5$), a diagram similar to Fig. 4 is often shown for the corner frequency f_c as a function of M_0 (Mayeda and Malagnini, 2007). To facilitate comparison of Fig. 4 with such corner frequency diagrams, the scaling laws for the corner frequency and the centroid time-delay are discussed in the next paragraph.

If the centroid time-delay τ_c is taken as a proxy for the half-duration t_h (i.e., $\tau_c = t_h$), the spectrum of the triangular moment rate function (MRF) assumed in GCMT and WCMT inversions can be written as

$$\hat{m}(f) = M_0 \left[\frac{\sin(\pi f \tau_c)}{\pi f \tau_c} \right]^2, \quad (2)$$

where f is frequency and M_0 is the seismic moment. The corner frequency f_c for the moment rate spectrum (Eq. (2)) is given by

$$f_c = \frac{1}{\pi \tau_c}. \quad (3)$$

Before 2004, the MRF used in GCMT inversions was modeled as a boxcar, for which the spectrum decays as f^{-1} at high frequency in contrast to the f^{-2} decay for the triangular MRF. The corner frequency for a boxcar MRF spectrum is, however, identical to that of the triangular MRF (i.e., $f_c = 1/\pi\tau_c$). The corner frequency f_c for a Brune-type scaling relation is given by (Brune, 1971, 1970)

$$f_c = c_1 \beta \left(\frac{\Delta\sigma}{M_0} \right)^{1/3} \quad (4)$$

where c_1 is a scaling parameter, β is a representative shear wave speed and $\Delta\sigma$ is a reference scaling parameter with units of stress. The scaling constant in Brune's model is $c_1 = 0.49$ (if all quantities are in c.g.s. units). We might call $\Delta\sigma$ a stress parameter as proposed, for example, by Boore (1983). The stress parameter $\Delta\sigma$ is not the stress drop of the earthquake, but in studies of small earthquakes where the assumptions of a circular fault and a constant rupture speed are considered approximately valid, it is often used as a proxy for the earthquake stress drop. For the large earthquakes discussed in this paper, the stress drop depends on the geometry of the fault and the slip distribution, and cannot be approximated by the stress parameter. Combining Eqs. (3) and (4), we obtain

$$\tau_c = \frac{1}{c_1 \pi \beta} \left(\frac{M_0}{\Delta\sigma} \right)^{1/3}. \quad (5)$$

Comparing this with Eq. (1) and assuming $\beta = 3.5$ km/s, we find that the stress parameter $\Delta\sigma$ for our data set is $\Delta\sigma \equiv \Delta\sigma_r = 3.7$ bar (0.37 MPa).

In Fig. 4, the stress parameter ratio $\Delta\sigma/\Delta\sigma_r = (\tau_r/\tau_c)^3$ is indicated for reference. The stress parameter $\Delta\sigma$ varies mainly over 2 orders of magnitude, which is smaller than the 3–4 orders of magnitude variability observed for stress-drop measurements from corner frequencies (Allmann and Shearer, 2009; Shearer et al., 2006). Events identified previously in Fig. 3 are also visible here:

(1) Tsunami earthquakes such as the 1992 Nicaragua earthquake and the 2006 Java earthquake.
(2) The $M_w = 6.7$ 2002 Guerrero earthquake on April 18 can also be easily identified with a value of $\tau_c/\tau_r \sim 5$.
(3) Earthquakes showing complicated rupture process such as the 2001 Kokoxili earthquake and the 2010 El-Mayor–Cucapah event.

Earthquakes associated with small values of τ_c/τ_r or large stress parameter ratios $\Delta\sigma/\Delta\sigma_r$ can also be identified in Fig. 4. Such temporally compact events can possibly be associated with high stress drop, as is certainly the case for the 2005 Tarapacá earthquake (Kuge et al., 2010). Since all events with $\tau_c/\tau_r < 0.46$ (i.e., red circles for $\Delta\sigma/\Delta\sigma_r > 10$) correspond to intermediate to large depth earthquakes, another possible explanation is an effect of the increase of shear wave velocity (β) with depth as suggested previously by Vidale and Houston (1993). This is illustrated in Fig. 5a, on which we see that most events with depth larger than 80 km (i.e., below the lithosphere) correspond, in average, to relatively small values of τ_c/τ_r. To remove this effect, we can use PREM velocities (Dziewonski and Anderson, 1981) in Eq. (5) to adjust τ_r for intermediate to large depth events. The resulting corrected τ_c/τ_r ratios, shown in Fig. 5b, suggest that the τ_c/τ_r decrease seen in Fig. 5a (i.e., assuming $\beta = 3.5$ km/s) can be explained by the increase of β as a function of depth.

Another class of events that clearly stands out in Fig. 4 is oceanic transform strike-slip earthquakes such as the 2003 Carlsberg ridge earthquake ($M_w = 7.6$). The normalized time-delays τ_c/τ_r obtained for strike-slip earthquakes are presented in Fig. 6. In this figure we see that events showing anomalously large values of τ_c/τ_r are generally oceanic fracture zone earthquakes. This observation is consistent with observations from Pérez-Campos et al. (2003), who report some anomalous oceanic strike-slip events with large time-delays compared to their seismic moment. Using techniques developed initially by Silver and Jordan (1983), anomalously long rupture processes are also reported by Ihmlé and Jordan (1994) and McGuire et al. (1996), who interpret these observations as slow precursory slip preceding some oceanic fracture zone earthquakes. This interpretation is, however, disputed by Abercrombie and Ekström (2003, 2001) because of large uncertainties due to mismodeling (epicenter mislocation, inaccuracy of the Earth model, etc.). Likewise, the large positive centroid time-delays measured at long-period do not support such slow slip precursors but rather abnormal long rupture durations. Consistent with Beroza and Jordan (1990), Pérez-Campos et al. (2003) describe these long-duration oceanic earthquakes as having anomalously low

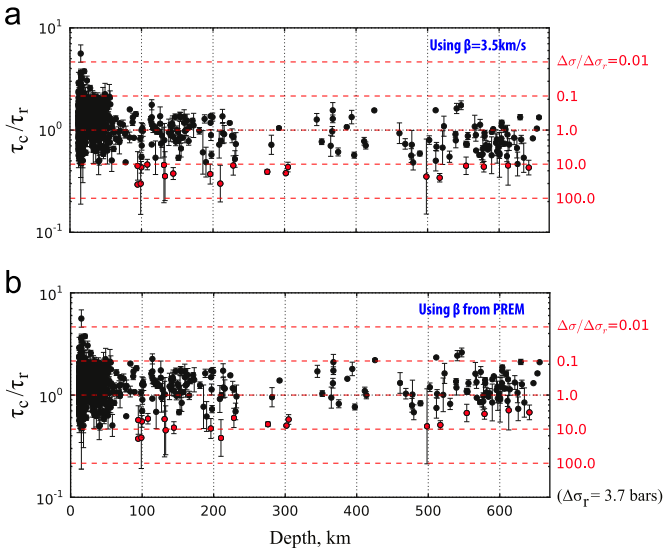

Fig. 5. Ratios τ_c/τ_r of observed time-delays τ_c to predictions τ_r for $M_0 \geq 6.5$ earthquakes from 1990 to 2012. The relative time-delays τ_c/τ_r are depicted (a) using $\tau_r = 1.2 \times 10^{-8} \times M_0^{1/3}$ (i.e., $\beta = 3.5$ km/s) and (b) by correcting τ_r from the shear-velocity variations as a function of depth (using values of β from the PREM model). Circles correspond to the geometric mean between GCMT and WCMT observations while error bars represent the deviation between GCMT and WCMT measurements for each earthquake. Red circles indicates events for which $\Delta\sigma/\Delta\sigma_r > 10$ in (a) and Fig. 4. (For interpretation of the references to color in this figure legend, the reader is referred to the web version of this article.)

Please cite this article as: Duputel, Z., et al., Using centroid time-delays to characterize source durations and identify earthquakes with unique characteristics. Earth and Planetary Science Letters (2013), http://dx.doi.org/10.1016/j.epsl.2013.05.024

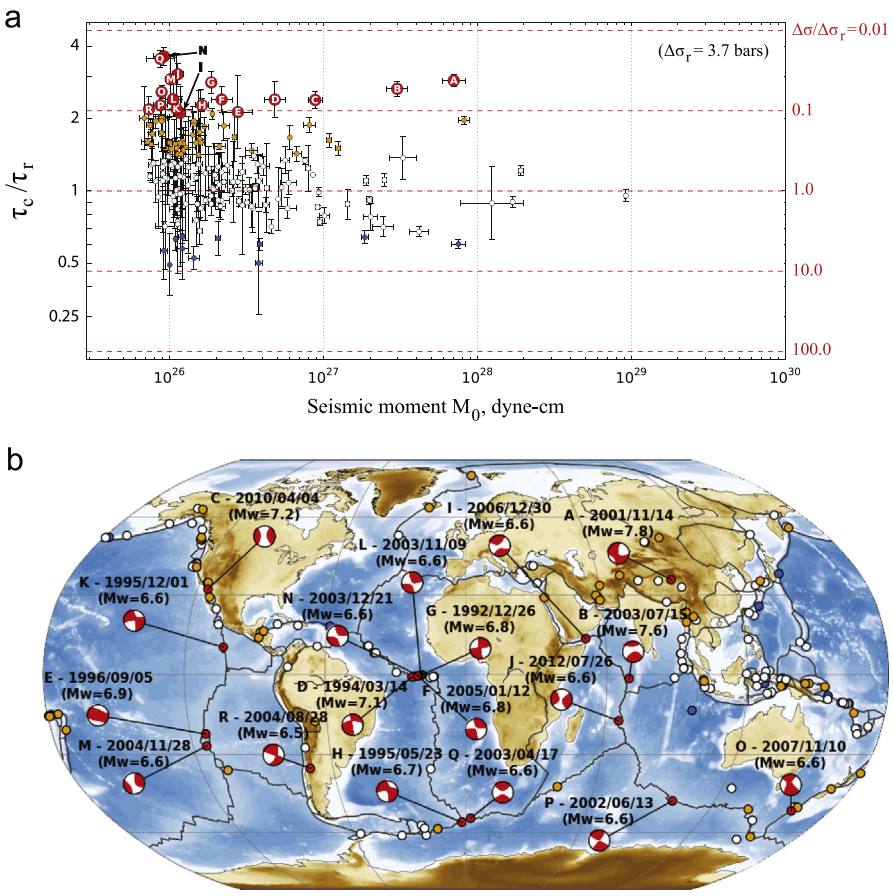

Fig. 6. Normalized time-delays τ_c/τ_r for strike-slip earthquakes for the events which occurred during the period from 1990 to 2012. (a) Similar to Fig. 4a but for strike-slip events only. (b) Map of normalized time-delays τ_c/τ_r for strike-slip earthquakes. Mechanisms with $\Delta\sigma/\Delta\sigma_r < 0.1$ bar identified with letters in (a) are shown. Circles in (a) and (b) are colored as a function of the stress parameter ratio $\Delta\sigma/\Delta\sigma_r$. (For interpretation of the references to color in this figure legend, the reader is referred to the web version of this article.)

apparent stresses as a consequence of slow rupture processes. Contrary to these observations, Choy and Boatwright (1995) and Choy and McGarr (2002) report high apparent stresses for oceanic transform zone earthquakes. Unfortunately, observations based on body-waves are subject to considerable uncertainties because of near-nodal take-off angles of body waves for strike-slip earthquakes (Schramm and Stein, 2009). The long rupture duration for some fracture zone earthquakes is, however, supported here by both W phase (WCMT) and fundamental-mode surface wave (GCMT) centroid time-delay measurements. Consistent with these observations, the finite-fault model obtained by Antolik et al. (2006) for the $M_w = 7.6$ Carlsberg ridge earthquake shows a long rupture process. Instead of a slow rupture component, the results of Antolik et al. (2006) indicate that this long duration is simply due to a very long rupture length. The finite-fault model proposed by Abercrombie and Ekström (2001) for the 1994 Romanche earthquake ($M_w = 7.1$) also shows an elongated rupture process involving normal or even high rupture velocities. These unusual aspect ratios can be explained by the location of these events on active ridges, where the seismogenic zone is restricted to very shallow depths because of the high temperature of the oceanic lithosphere. Such elongated rupture scenarios are consistent with large time-delay estimates that are mostly controlled by the fault length. This interpretation of elongated ruptures is also compatible with large corner frequencies and high stress drop observations reported by Allmann and Shearer (2009) that are most sensitive to the fault width (which can be small if the seismogenic zone is restricted to shallow depths).

6. Conclusions

In this short note, we show that the centroid time-delay provides a very straightforward and reliable estimate of the rupture duration. In some cases, such as for long-tailed moment-rate functions, the centroid time-delay provides a more meaningful way of quantifying the sources' temporal characteristics than other possible definitions of duration. We also present a simple scaling relationship between the seismic moment and the centroid time-delay, both of which can be determined accurately and objectively from the analysis of long-period seismic waves. This standard scaling relationship can be used to estimate the variability of the stress parameter and to identify events with unique source properties. Different types of unusual earthquakes can be identified from their anomalous centroid time-delays. First of all, events involving slow rupture processes, such as tsunami earthquakes, generally show larger centroid time-delay estimates than expected from their seismic moments (e.g., the 2006 Java event). Secondly, anomalous time-delays can also be observed for events with unusual aspect ratios. For instance, some oceanic fracture zone earthquakes involving elongated faults but ordinary rupture velocities can be associated with anomalously long time-delays (e.g., the 2003 Carlsberg ridge earthquake). Thirdly, high or low stress-drop earthquakes can induce significant time-delay variations. For example, high stress drop events can have small centroid time-shifts because these earthquakes generally have a temporally compact moment rate function (e.g., the 2011 Tohoku-oki earthquake). Also, earthquakes with complicated ruptures involving multiple sub-events, which often have a large moment

Please cite this article as: Duputel, Z., et al., Using centroid time-delays to characterize source durations and identify earthquakes with unique characteristics. Earth and Planetary Science Letters (2013), http://dx.doi.org/10.1016/j.epsl.2013.05.024

rate at a late stage of faulting, tend to have large time-shifts (e.g., the 2002 Denali earthquake). Despite these various interpretations for rupture duration anomalies, the centroid time-delay/moment scaling relation is useful for identifying events with unusual characteristics. In this study, many interesting events, which have been debated in earthquake seismology for the last 2 decades, have been identified using this approach. This very simple and straightforward analysis also has practical applications, such as the rapid identification of tsunami earthquakes in real-time.

Acknowledgments

We thank Zhongwen Zhan, Gavin Hayes, Göran Ekström and an anonymous reviewer for their helpful suggestions. This work uses Federation of Digital Seismic Networks (FDSN) seismic data, CMT solutions from the Global CMT catalog and event origin times from the USGS PDE catalog. The Incorporated Research Institutions for Seismology (IRIS) Data Management System (DMS) was used to access the data. This work made use of the Matplotlib python library created by John D. Hunter.

Appendix A. Supplementary material

Supplementary data associated with this article can be found in the online version at http://dx.doi.org/10.1016/j.epsl.2013.05.024.

References

Abercrombie, R.E., Antolik, M., Ekström, G., 2003. The June 2000 Mw7.9 earthquakes south of Sumatra: deformation in the India–Australia Plate. J. Geophys. Res. 108, 2018.

Abercrombie, R.E., Antolik, M., Felzer, K., Ekström, G., 2001. The 1994 Java tsunami earthquake—slip over a subducting seamount. J. Geophys. Res. 106, 6595–6607.

Abercrombie, R.E., Ekström, G., 2001. Earthquake slip on oceanic transform faults. Nature 410, 74–77.

Abercrombie, R.E., Ekström, G., 2003. A reassessment of the rupture characteristics of oceanic transform earthquakes. J. Geophys. Res. 108, 2225.

Aki, K., 1967. Scaling law of seismic spectrum. J. Geophys. Res. 72, 1217.

Aki, K., 1972. Earthquake mechanism. Tectonophysics 13, 423–446.

Allmann, B.P., Shearer, P.M., 2009. Global variations of stress drop for moderate to large earthquakes. J. Geophys. Res. 114, B01310.

Ammon, C.J., Chen, J., Thio, H.K., Robinson, D., Ni, S., Hjörleifsdóttir, V., Kanamori, H., Lay, T., Das, S., Helmberger, D., Ichinoise, G., Polet, J., Wald, D., 2005. Rupture process of the 2004 Sumatra–Andaman earthquake. Science 308, 1133–1139.

Ammon, C.J., Lay, T., Velasco, A.A., Kanamori, H., 2006. The 17 July 2006 Java tsunami earthquake. Geophys. Res. Lett. 33, L24308.

Antolik, M., Abercrombie, R.E., Pan, J., Ekström, G., 2006. Rupture characteristics of the 2003 Mw 7.6 mid-Indian Ocean earthquake: implications for seismic properties of young oceanic lithosphere. J. Geophys. Res. 111, B04302.

Beroza, G.C., Jordan, T.H., 1990. Searching for slow and silent earthquakes using free oscillations. J. Geophys. Res. 95, 2485.

Boore, D.M., 1983. Stochastic simulation of high-frequency ground motions based on seismological models of the radiated spectra. Bull. Seismol. Soc. Am 73, 1865–1894.

Brune, J.N., 1970. Tectonic stress and the spectra of seismic shear waves from earthquakes. J. Geophys. Res 75, 4997–5009.

Brune, J.N., 1971. Correction to tectonic stress and the spectra of seismic shear waves from earthquakes. J. Geophys. Res. 76, 5002.

Choy, G.L., Boatwright, J.L., 1995. Global patterns of radiated seismic energy and apparent stress. J. Geophys. Res. 100, 18205–18228.

Choy, G.L., McGarr, A., 2002. Strike-slip earthquakes in the oceanic lithosphere: observations of exceptionally high apparent stress. Geophys. J. Int. 150, 506–523.

Duputel, Z., Rivera, L., Kanamori, H., Hayes, G., 2012. W phase source inversion for moderate to large earthquakes (1990–2010). Geophys. J. Int. 189, 1125–1147.

Dziewonski, A., Chou, T.A., Woodhouse, J.H., 1981. Determination of earthquake source parameters from waveform data for studies of global and regional seismicity. J. Geophys. Res. 86, 2825–2852.

Dziewonski, A.M., Anderson, D.L., 1981. Preliminary reference Earth model. Phys. Earth Planet. Inter. 25, 297–356.

Dziewonski, A.M., Woodhouse, J.H., 1983. An experiment in systematic study of global seismicity: centroid-moment tensor solutions for 201 moderate and large earthquakes of 1981. J. Geophys. Res. 88, 3247.

Earthquake Research Institute (ERI), 2000. EIC Seismological Note 94.

Eberhart-Phillips, D., Haeussler, P.J., Freymueller, J.T., Frankel, A.D., Rubin, C.M., Craw, P., Ratchkovski, N.A., Anderson, G., Carver, G.A., Crone, A.J., Dawson, T.E., Fletcher, H., Hansen, R., Harp, E.L., Harris, R.A., Hill, D.P., Hreinsdóttir, S., Jibson, R.W., Jones, L.M., Kayen, R., Keefer, D.K., Larsen, C.F., Moran, S.C., Personius, S.F., Plafker, G., Sherrod, B., Sieh, K., Sitar, N., Wallace, W.K., 2003. The 2002 Denali Fault Earthquake, Alaska: a large magnitude, slip-partitioned event. Science, 300; pp. 1113–1118.

Ekström, G., 1989. A very broad band inversion method for the recovery of earthquake source parameters. Tectonophysics 166, 73–100.

Ekström, G., Engdahl, E.R., 1989. Earthquake source parameters and stress distribution in the Adak Island region of the central Aleutian Islands, Alaska. J. Geophys. Res. 94, 15499.

Ekström, G., Nettles, M., Dziewonski, A.M., 2012. The global CMT project 2004–2010: centroid-moment tensors for 13,017 earthquakes. Phys. Earth Planet. Inter. 200–201, 1–9.

Hauksson, E., Stock, J., Hutton, K., Yang, W., Vidal-Villegas, J.A., Kanamori, H., 2010. The 2010 Mw7.2 El Mayor–Cucapah Earthquake Sequence, Baja California, Mexico and Southernmost California, USA: active seismotectonics along the Mexican Pacific Margin. Pure Appl. Geophys. 168, 1255–1277.

Heinrich, P., Piatanesi, A., Okal, E.A., Hébert, H., 2000. Near-field modeling of the July 17, 1998 tsunami in Papua New Guinea. Geophys. Res. Lett. 27, 3037–3040.

Heki, K., Miyazaki, S., Tsuji, H., 1997. Silent fault slip following an interplate thrust earthquake at the Japan Trench. Nature 386, 595–598.

Hidayat, D., Barker, J.S., Satake, K., 1995. Modeling the seismic source and tsunami generation of the December 12, 1992 Flores Island, Indonesia, earthquake. Pure Appl. Geophys. 144, 537–554.

Hill, E.M., Borrero, J.C., Huang, Z., Qiu, Q., Banerjee, P., Natawidjaja, D.H., Elosegui, P., Fritz, H.M., Suwargadi, B.W., Pranantyo, I.R., Li, L., Macpherson, K.A., Skanavis, V., Synolakis, C.E., Sieh, K., 2012. The 2010 Mw 7.8 Mentawai earthquake: very shallow source of a rare tsunami earthquake determined from tsunami field survey and near-field GPS data. J. Geophys. Res.: Solid Earth 117, B06402.

Houston, H., Benz, H.M., Vidale, J.E., 1998. Time functions of deep earthquakes from broadband and short-period stacks. J. Geophys. Res. 103, 29895.

Iglesias, A., Singh, S.K., Pacheco, J.F., Alcántara, L., Ortiz, M., Ordaz, M., 2003. Near-trench Mexican Earthquakes have anomalously low peak accelerations. Bull. Seismol. Soc. Am. 93, 953–959.

Ihmlé, P.F., Jordan, T.H., 1994. Teleseismic search for slow precursors to large earthquakes. Science 266, 1547–1551.

Ihmlé, P.F., Gomez, J.-M., Heinrich, P., Guibourg, S., 1998. The 1996 Peru tsunamigenic earthquake: broadband source process. Geophys. Res. Lett. 25, 2691.

Ishii, M., Shearer, P.M., Houston, H., Vidale, J.E., 2005. Extent, duration and speed of the 2004 Sumatra–Andaman earthquake imaged by the Hi-Net array. Nature 435, 933–936.

Kanamori, H., 1972. Mechanism of tsunami earthquakes. Phys. Earth Planet. Inter. 6, 356–359.

Kanamori, H., Anderson, D.L., 1975. Theoretical basis of some empirical relations in seismology. Bull. Seismol. Soc. Am. 65, 1073–1095.

Kanamori, H., Given, J.W., 1981. Use of long-period surface waves for rapid determination of earthquake-source parameters. Phys. Earth Planet. Inter. 27, 8–31.

Kanamori, H., Kikuchi, M., 1993. The 1992 Nicaragua earthquake: a slow tsunami earthquake associated with subducted sediments. Nature 361, 714–716.

Kanamori, H., Rivera, L., 2008. Source inversion of W phase: speeding up seismic tsunami warning. Geophys. J. Int. 175, 222–238.

Kaverina, A., Dreger, D., Antolik, M., 1998. Source process of the 21 April, 1997 Santa Cruz Island Earthquake (Mw7.8). Geophys. Res. Lett. 25, 4027.

Kikuchi, M., Kanamori, H., 1995. The Shikotan Earthquake of October 4, 1994: lithospheric earthquake. Geophys. Res. Lett. 22, 1025–1028.

Kostoglodov, V., Singh, S.K., Santiago, J.A., Franco, S.I., Larson, K.M., Lowry, A.R., Bilham, R., 2003. A large silent earthquake in the Guerrero seismic gap, Mexico. Geophys. Res. Lett. 30, 1807.

Kuge, K., Kase, Y., Urata, Y., Campos, J., Perez, A., 2010. Rupture characteristics of the 2005 Tarapaca, northern Chile, intermediate-depth earthquake: evidence for heterogeneous fluid distribution across the subducting oceanic plate? J. Geophys. Res. 115, B09305.

Lambotte, S., Rivera, L., Hinderer, J., 2006. Rupture length and duration of the 2004 Aceh-Sumatra earthquake from the phases of the Earth's gravest free oscillations. Geophys. Res. Lett. 33, L03307.

Lay, T., Ammon, C.J., Hutko, A.R., Kanamori, H., 2010a. Effects of Kinematic Constraints on Teleseismic Finite-Source Rupture Inversions: Great Peruvian Earthquakes of 23 June 2001 and 15 August 2007. Bull. Seismol. Soc. Am. 100, 969–994.

Lay, T., Ammon, C.J., Kanamori, H., Koper, K.D., Sufri, O., Hutko, A.R., 2010b. Teleseismic inversion for rupture process of the 27 February 2010 Chile (Mw8.8) earthquake. Geophys. Res. Lett. 37, L13301.

Lay, T., Ammon, C.J., Kanamori, H., Rivera, L., Koper, K., Hutko, A.R., 2010c. The 2009 Samoa–Tonga great earthquake triggered doublet. Nature 466, 964–968.

Lay, T., Ammon, C.J., Kanamori, H., Yamazaki, Y., Cheung, K.F., Hutko, A.R., 2011. The 25 October 2010 Mentawai tsunami earthquake (Mw 7.8) and the tsunami hazard presented by shallow megathrust ruptures. Geophys. Res. Lett. 38, L06302.

Lay, T., Kanamori, H., 2011. Insights from the great 2011 Japan earthquake. Phys. Today 64, 33–39.

Lay, T., Kanamori, H., Ammon, C.J., Hutko, A.R., Furlong, K., Rivera, L., 2009. The 2006–2007 Kuril Islands great earthquake sequence. J. Geophys. Res. 114, B11308.

Please cite this article as: Duputel, Z., et al., Using centroid time-delays to characterize source durations and identify earthquakes with unique characteristics. Earth and Planetary Science Letters (2013), http://dx.doi.org/10.1016/j.epsl.2013.05.024

Mayeda, K., Malagnini, L., 2007. A new spectral ratio method using narrow band coda envelopes: evidence for non-self-similarity in the Hector Mine sequence. Geophys. Res. Lett 34, L11303.
McGuire, J.J., Ihmlé, P.F., Jordan, T.H., 1996. Time-domain observations of a slow precursor to the 1994 Romanche Transform Earthquake. Science 274, 82–85.
Nakayama, W., Takeo, M., 1997. Slip history of the 1994 Sanriku-Haruka-Oki, Japan, earthquake deduced from strong-motion data. Bull. Seismol. Soc. Am. 87, 918–931.
Newman, A., Hayes, G., Wei, Y., Convers, J., 2011. The 25 October 2010 Mentawai tsunami earthquake, from real-time discriminants, finite-fault rupture, and tsunami excitation. Geophys. Res. Lett. 38, L05302.
Newman, A.V., Okal, E.A., 1998. Teleseismic estimates of radiated seismic energy: the E/M0 discriminant for tsunami earthquakes. J. Geophys. Res. 103, 26885.
Park, S.-C., Mori, J., 2007. Triggering of earthquakes during the 2000 Papua New Guinea earthquake sequence. J. Geophys. Res. 112, B03302.
Pérez-Campos, X., McGuire, J.J., Beroza, G.C., 2003. Resolution of the slow earthquake/high apparent stress paradox for oceanic transform fault earthquakes. J. Geophys. Res. 108, 2444.
Polet, J., Kanamori, H., 2000. Shallow subduction zone earthquakes and their tsunamigenic potential. Geophys. J. Int. 142, 684–702.
Polet, J., Thio, H.K., 2003. The 1994 Java tsunami earthquake and its "Normal" aftershocks. Geophys. Res. Lett. 30, 1474.
Romanowicz, B., 1992. Strike-slip earthquakes on quasi-vertical transcurrent faults: inferences for general scaling relations. Geophys. Res. Lett. 19, 481–484.
Satake, K., 1994. Mechanism of the 1992 Nicaragua tsunami earthquake. Geophys. Res. Lett. 21, 2519–2522.
Scholz, C.H., 1982. Scaling laws for large earthquakes: consequences for physical models. Bull. Seismol. Soc. Am. 72, 1–14.
Schramm, K., Stein, S., 2009. Apparent slow oceanic transform earthquakes due to source mechanism bias. Seismol. Res. Lett. 80, 102–107.
Shearer, P.M., Prieto, G.A., Hauksson, E., 2006. Comprehensive analysis of earthquake source spectra in southern California. J. Geophys. Res. 111, B06303.
Silver, P.G., Jordan, T.H., 1983. Total-moment spectra of fourteen large earthquakes. J. Geophys. Res. 88, 3273.
Sladen, A., 2007a. Tectonics Observatory Source Models of Large Earthquakes—August/15/2007 (Mw 8.0), Peru http://www.tectonics.caltech.edu/slip_history.
Sladen, A., 2007b. Tectonics Observatory Source Models of Large Earthquakes—September/12/2007 (Mw 8.4), South Sumatra, http://www.tectonics.caltech.edu/slip_history.
Sladen, A., 2008a. Tectonics Observatory Source Models of Large Earthquakes—May/12/2008 (Mw 7.9), East Sichuan, http://www.tectonics.caltech.edu/slip_history.
Sladen, A., 2008b. Tectonics Observatory Source Models of Large Earthquakes—November/16/2008 (Mw 7.3), Sulawesi, http://www.tectonics.caltech.edu/slip_history.
Sladen, A., 2009a. Tectonics Observatory Source Models of Large Earthquakes—October/07/2009 (Mw 7.6), Vanuatu, http://www.tectonics.caltech.edu/slip_history.
Sladen, A., 2009b. Tectonics Observatory Source Models of Large Earthquakes—September/30/2009 (Mw 7.6), Padang, http://www.tectonics.caltech.edu/slip_history.
Sladen, A., Tavera, H., Simons, M., Avouac, J., 2010. Source model of the 2007 Mw 8.0 Pisco, Peru earthquake: implications for seismogenic behavior of subduction megathrusts. J. Geophys. Res. 114, B02405.
Smith, G.P., Ekström, G., 1995. Using travel-time and waveform data to study the earthquake source. AGU Fall Meeting Abstracts, EOS Supplement 76, 389.
Synolakis, C.E., Bardet, J.P., Borrero, J.C., Davies, H.L., Okal, E.A., Silver, E.A., Sweet, S., Tappin, D.R., 2002. The slump origin of the 1998 Papua New Guinea Tsunami. Proc. R. Soc. A: Math. Phys. Eng. Sci. 458, 763–789.
Tanioka, Y., Ruff, L., Satake, K., 1996. The Sanriku-Oki, Japan, Earthquake of December 28, 1994 (Mw7.7): rupture of a different asperity from a previous earthquake. Geophys. Res. Lett. 23, 1465.
Tanioka, Y., Ruff, L.J., 1997. Source time functions. Seismol. Res. Lett. 68, 386–400.
Tocheport, A., Rivera, L., Van der Woerd, J., 2006. A study of the 14 November 2001 Kokoxili Earthquake: history and geometry of the rupture from teleseismic data and field observations. Bull. Seismol. Soc. Am. 96, 1729–1741.
Tsai, V.C., Nettles, M., Ekström, G., Dziewonski, A.M., 2005. Multiple CMT source analysis of the 2004 Sumatra earthquake. Geophys. Res. Lett. 32, L17304.
Tsuji, Y., Matsutomi, H., Imamura, F., Takeo, M., Kawata, Y., Matsuyama, M., Takahashi, T., Sunarjo, Harjadi, P., 1995. Damage to coastal villages due to the 1992 Flores Island earthquake tsunami. Pure Appl. Geophys. 144, 481–524.
Vidale, J.E., Houston, H., 1993. The depth dependence of earthquake duration and implications for rupture mechanisms. Nature 365, 45–47.
Wielandt, E., Steim, J.M., 1986. A digital very-broad-band seismograph. Ann. Geophys. Ser. 4, 227–232.
Wielandt, E., Streckeisen, G., 1982. The leaf-spring seismometer: design and performance. Bull. Seismol. Soc. Am. 72, 2349.
Yagi, Y., 2002. 2002 Northen Sumatra, Indonesia Earthquake, http://iisee.kenken.go.jp/staff/yagi.
Yagi, Y., 2003. Source process of large and significant earthquakes in 2003. Bull. Int. Inst. Seismol. Earthquake Eng., 145–153.
Yagi, Y., 2004. Source rupture process of the 2003 Tokachi-oki earthquake determined by joint inversion of teleseismic body wave and strong ground motion data. Earth Planets Space 56, 311–316.

Please cite this article as: Duputel, Z., et al., Using centroid time-delays to characterize source durations and identify earthquakes with unique characteristics. Earth and Planetary Science Letters (2013), http://dx.doi.org/10.1016/j.epsl.2013.05.024